JOURNAL OF THERMOPHYSICS AND HEAT TRANSFER
Vol. 9, No. 4, October–December 1995

Nose Cavity Effects on Blunt Body Pressure and Temperatures at Mach 5

K. B. Yüceil* and D. S. Dolling†
University of Texas at Austin, Austin, Texas 78712

Surface temperatures on a hemisphere-cylinder body with a nose cavity in a Mach 4.9 airflow have been measured using an infrared camera. Fluctuating surface pressures have also been measured at the cavity base. The cavity diameter D was fixed at one-half the cylinder diameter and the length L of the cavity was varied. If the cavity lip is sharp and the cavity is "shallow" ($0.15 \leq L/D \leq 0.35$) or "very deep" ($L/D \geq 1$) an axisymmetric, nominally steady "cool ring" forms on the external surface downstream of the lip. Flow visualization shows that the cool ring is caused by separation at the lip. Rounding the cavity lip eliminates or reduces separation and temperatures return to levels characteristic of the model without the cavity. For "intermediate deep" cavities ($0.40 \leq L/D \leq 0.70$) the cavity pressure signals switch from a low-amplitude to high-amplitude level at random intervals resulting in an unstable, nonaxisymmetric temperature field downstream of the lip. Changes in cavity base shape from spherical to flat have little effect on the temperature history for shallow and very deep cavities, whereas for intermediate depth cavities the effects are more significant.

Introduction

THE U.S. Army is very interested in the development of hypervelocity projectiles because they have substantially larger penetration depths[1,2] due to their very high kinetic energy at impact. However, in the range of interest (2–4 km/s), the projectile nose experiences very high heating rates, and the resulting ablation can produce unacceptable perturbations in the aerodynamics and the flight path. As an example of the severity of the heating, the stagnation temperature attained at sea level and a velocity of about 2.6 km/s (Mach 7.6) corresponds to the melting point of tungsten (3683 K). There is consequently a need to develop active or passive techniques to reduce tip heating rates.

It was reported[3] more than 30 years ago that the stagnation point heat transfer rate for a concave axisymmetric nose cone at supersonic Mach numbers is considerably lower than that of a convex nose cone. More recently, the flow physics associated with a nose cavity at Mach 10 have been documented.[4–7] Huebner and Utreja[4] have shown that for this nose cavity configuration the heat transfer rate at the cavity base is less than that at the rim of the nose. They also noted that the bow-shock oscillation frequency and amplitude were directly related to the cavity depth. In numerical and experimental studies, Sambamurthi et al.[5] obtained a good correlation between computational results and wind-tunnel data for the unsteady nature of the shock and the pressure distribution on the cavity wall for this configuration. Marquart et al.[6] focused on the dynamics of the detached bow shock and the acoustic resonance in the forward-facing nose cavity of a blunt-faced model and found that the primary mode of pressure oscillation in the cavity is at the classic organ-pipe frequency, and that the rms levels of the fluctuating pressure along the cavity wall increased toward the base. Huebner and Utreja[7] presented a detailed description of the bow-shock behavior associated with a conical-walled cavity with a flat circular base. They observed that the primary behavior was a stable, periodically oscillating bow shock, although a violent bow-shock instability occurred for one set of conditions during the test.

The general objective of the study described in this article was to determine if a nose cavity can reduce the maximum surface temperatures in the vicinity of the nose tip. Prior to the present test program some preliminary information on the effects of the cavity was obtained using a thermal imaging system. A detailed description of the system and the preliminary results can be found in Yuceil et al.[8] Thermal imaging has the advantage of being nonintrusive, and a large volume of data can be acquired with relatively little effort. In those initial experiments, only changes in cavity length L and diameter D were considered. It was found that shallower cavities ($L/D \leq 0.35$) with large diameters had a stable cool ring. The cool ring is a region on the surface in the vicinity of the cavity lip in which temperatures are lower than those of a plain spherical nose. Fluctuating pressure measurements made at the center of the cavity base showed that oscillations inside the cavity had dominant frequencies that were close to classic organ pipe values.

The current study presents results from a more detailed set of experiments made to explore the physical causes of the cool ring and to examine the sensitivity of earlier results to changes in cavity lip and base shape. In these experiments, cavity depths that were close to those of earlier tests have been studied, as well as much deeper cavities. Surface temperature and fluctuating wall pressure measurements have been made, as well as surface flow visualization.

Experimental Arrangement

Wind-Tunnel and Models

Experiments were conducted in the Mach 5 blowdown wind tunnel of the University of Texas at Austin. The tunnel was operated at a stagnation pressure and temperature of 2.275 MPa (330 psia) and 370–375 K, respectively. At a freestream Mach number of 4.9 these conditions generate a freestream Reynolds number of 48.5×10^6/m (1.48×10^7/ft). Run times are about 30 s. The test section is 17.78 cm high by 15.24 cm wide (7 by 6 in.) and has two circular observation windows.

The model was a hemispherically blunted cylinder, 5.08 cm (2 in.) in diameter, with a variable-length cavity at the tip (Fig. 1). The cavity diameter was 2.54 cm (1.0 in.) for most

Received Oct. 13, 1994; revision received April 14, 1995; accepted for publication April 19, 1995.

*Graduate Research Assistant, Center for Aeromechanics Research, Department of Aerospace Engineering and Engineering Mechanics. Student Member AIAA.

†Professor, Center for Aeromechanics Research, Department of Aerospace Engineering and Engineering Mechanics. Associate Fellow AIAA.

Table 1 Cavity sizes used in experiments

Cavity geometry			*L/D*	
Base	Lip	Shallow	Deep	Very deep
Spherical	Sharp	0.21	0.54	1.19
		(0.25)	(0.57)	(1.22)
Spherical	Round	0.14	0.485	1.13
		(0.185)	(0.51)	(1.15)
Flat	Sharp	0.235	0.59	——
		(0.23)	(——)	(1.235)
Flat	Round	0.18	0.525	——
		(0.17)	(——)	(1.175)

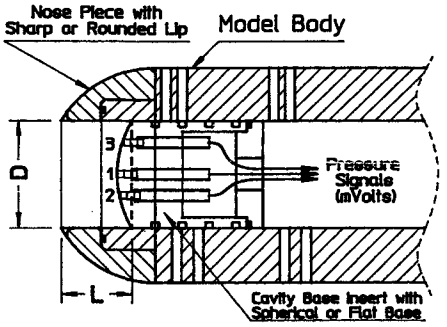

Fig. 1 Modular body design and fluctuating pressure instrumentation arrangement.

cases, however, some fluctuating pressure measurements were made for $D = 1.27$ cm (0.5 in.). In order to explore the effects of cavity lip and base geometry a modular model concept was adopted. Different nose and cavity base pieces (inserts) were used on the same model body as shown in Fig. 1. Nose pieces and inserts were made of polycarbonate in order to use them with the infrared (IR) camera system, as will be explained later. Inserts for pressure measurements were made from brass, as was the model body. Either of two nose pieces, one with sharp cavity lip and the other with ~1.5 mm lip radius, could be screwed into the model body to form the sphere–cylinder model. In addition, two inserts, one with a spherical end (having a radius equal to that of the hemisphere) and the other with a flat end could be fixed at discrete locations inside the cavity using set screw holes on the model body. Cavities are called (due to flow phenomena) shallow, deep, and very deep; the term shallow is used if $(L/D) < 0.40$, deep if $0.40 < (L/D) < 0.70$, and very deep if $(L/D) > 1.0$. By changing the axial position of the cavity insert (see Fig. 1) values of (L/D) ranging from 0 to 2.25 for temperature measurements, and 0 to 1.5 for pressure measurements could be obtained. The latter range was lower due to space constraints of installing pressure transducers. Table 1 gives the values of L/D for the IR camera experiments (values for the pressure tests are shown in parentheses). Note that L is defined in Fig. 1 as the distance from the cavity lip to the cavity base-side wall junction. Because of the different inserts used for pressure measurements, L/D values were slightly different from those for IR camera experiments.

To obtain accurate temperature measurements the model material must have properties close to that of a blackbody. Also, since the IR camera detects temperature differences between the target and the background, the thermal gradient at the model surface should be maximized. Thus, a material with a low thermal conductivity is required. Consequently, polycarbonate that has good structural properties and a very low thermal conductivity was selected as the material for the nose pieces.

Figure 1 also shows the insert instrumented for fluctuating pressure measurements. Three Kulite® dynamic pressure transducers (model XCQ-062-50A) with an effective frequency response of approximately 50 kHz and with a pressure range of 0–345 kPa (0–50 psia) were used. Measured pressures ranged from about 70–207 kPa (10–30 psia). The transducers are nominally 1.63 mm (0.064 in.) in diameter and were installed with their axes parallel to the model axis, and for the flat base with their faces flush with the surface. For the spherical base, off-center transducers were slightly recessed from the higher side of the transducer installation hole (see Fig. 1). The signals were amplified by EG&G Amplifiers and passed through Ithaco 4213 Electronic Filters with cutoff frequency set at 50 kHz. A LeCroy 6810 Waveform Recorder with 12-bit resolution digitized the signals and stored them in an internal buffer for transfer to an HP 9000 minicomputer. Most of the experiments were run at sampling rates of 1 MHz or 200 kHz. A total of 524,288 points spanning a real time of 2.62144 s for 200 kHz sampling rate, and 0.524288 s for 1 MHz sampling rate were taken per run. The data strings for each channel were broken into 512 records of 1024 data points and analyzed to obtain rms levels, cross correlations, power spectra, etc. Due to high time resolution of signals sampled at 1 MHz, highly resolved cross-correlation curves were obtained, whereas signals sampled at 200 kHz provided a resolution of 0.195 kHz in frequency for power spectra. Data were taken when the tunnel reached stable stagnation conditions, which occurred about 15–20 s after startup.

The model was installed on the centerline of the test section using a streamlined support attached to the tunnel floor (see Fig. 2). The viewing window was made of zinc selenide (for maximum transmission of IR radiation) and was on loan from NASA Langley Research Center.

Experimental Procedure

On tunnel startup, the stagnation temperature rises from approximately room temperature to close to the set point [about 372 K (210°F)] in about 15 s. During this period, the increase in model nose temperature per unit time is directly related to the tunnel stagnation temperature rise per unit time. To make meaningful comparative measurements of the rate of change of the model temperature with time, the ideal situation is for the tunnel to be at steady conditions before the model is subjected to the flow.

In the present study, shielding was used rather than injection of the model since the latter would require expensive modifications to the test section. The shielding method was relatively simple and required only an ordinary racquetball cut in half. This rubber cap fits snugly over the model nose. A line was attached to the model just behind the cap rim using a slipknot so that when the line was pulled the cap slid over the nose and flew off downstream. This rubber cap provided very good thermal insulation since the nose temperature

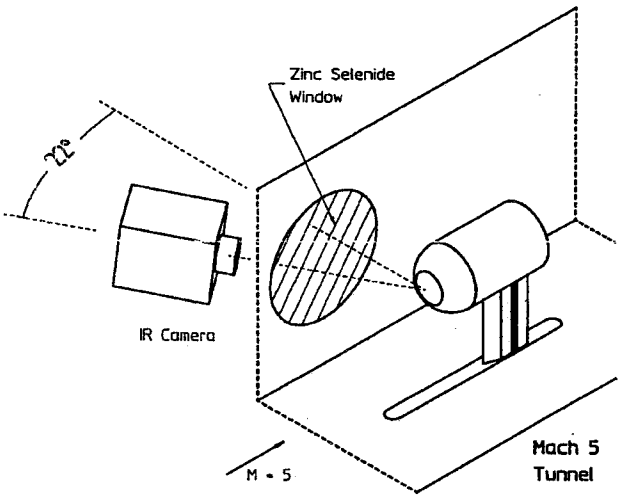

Fig. 2 Experimental setup.

rose only 2–3 K (4–5°F) over 20–30 s, whereas without the cap the rise would be around 65–70 K (120–130°F).

The IR video camera was operated continuously during the entire run. By matching the clocks on the camera and on the data acquisition system, the time when the cap came off could be determined within 0.02 s. The data prior to this time were discarded. For the fluctuating pressure measurements, shielding the model was unnecessary since the data could be recorded after the tunnel reached stable conditions.

Calibration Processes

The IR camera system has a factory-installed calibration lookup-curve in its control unit. Two parameters influencing the calibration are the transmittance of the zinc selenide window and the emissivity of the polycarbonate model surface. To estimate the former, a polycarbonate target mounted on a test stand was held at constant high temperature and viewed by the camera with and without the window. The transmittance of the window was found to be 64% in °F. To estimate the emissivity of the model, two thermocouples were attached to the surface of a flat polycarbonate target held at high temperature and the emissivity parameter was adjusted until the temperature values indicated by the thermocouples and camera were matched to better than 0.5 K (1°F). Over the temperature range to be measured the emittance was found to be 96% relative to that of a blackbody.

The temperature data acquisition and analysis system consists of an IBM compatible personal computer, a color graphics card, and a Thermoteknix ThermaGRAM card along with an RGB video monitor. The fastest approach to obtain temperature histories from the raw data on tape is the "snapshots" option in which the time interval between temperature readings is 1/60 s. Using this option, the history of the average temperature of up to three regions at a time can be displayed on the computer screen or recorded in a data file. These regions can be anywhere on the thermal image and their sizes can be varied from a single pixel up to rectangles or circles that include any number of pixels. In addition, data were further averaged in groups of 10 frames each to improve stability.

Temperature corrections due to viewing angle were made where necessary using the correction curves obtained experimentally. For viewing angles up to 40 deg to the surface normal, the radiation intensity did not change more than 1%, whereas after 50–60 deg it decreased dramatically. To account for this effect, a high-temperature, flat target was viewed at different angles and the variation of surface temperature was observed. Tests made at two different surface temperatures showed essentially the same variation with angle.[8]

For the fluctuating pressure measurements, the transducers were calibrated statically using a Heise pressure gauge. The signal-to-noise ratio (SNR) was determined experimentally and varied from 50:1 for low-amplitude oscillations to 350:1 for high-amplitude oscillations.

Discussion of Results

General Characteristics

As mentioned in the Introduction, preliminary experiments[8] with shallow cavities showed a reduction in temperature in the vicinity of the cavity lip due to the presence of a cool ring. Figure 3 shows some sample IR image photographs reproduced from the videos, which were taken approximately 15 s after the model nose was exposed to the flow. All cases shown are for spherical base and sharp cavity lip configuration. As can be seen by the dark band in the images in Figs. 3b and 3c, the cool ring starts at the cavity edge and extends downstream about 6–7 deg in terms of the angle measured from the model axis. For deep cavity cases (Figs. 3d and 3e), the cool ring cannot be observed and there are hot and cold spots on the surface in the vicinity of the lip. The flow in such cases

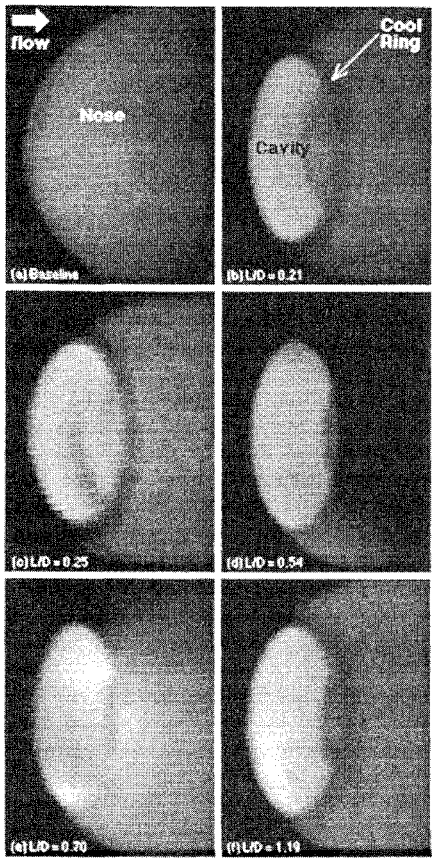

Fig. 3 Sample IR images for different cavity depths: a) baseline, b) L/D = 0.21, c) L/D = 0.25, d) L/D = 0.54, e) L/D = 0.70, and f) L/D = 1.19 (brighter regions indicate higher temperatures).

appears to be highly "unstable" and nonaxisymmetric as well as very sensitive to the changes in the cavity depth. In this context, unstable implies a flow switching randomly and rapidly between distinct states rather than oscillating within a narrow range of amplitudes at constant frequency. The subsequent lack of symmetry in the temperature field makes comparisons with axisymmetric cases difficult, and care must be taken in interpreting the results. As can be seen in Fig. 3d, L/D = 0.54 case has much lower surface temperatures indicated by the darker regions over almost the entire external surface, whereas L/D = 0.70 case (Fig. 3e) has a hot spot (brighter region) outside of the cavity, which makes it quite different from the L/D = 0.54 case. Although it cannot be seen in these still images, real-time playbacks of these deep cavity cases show unstable and oscillating temperature fields in and around the cavity, and this can also be observed in the surface temperature histories of some of the cases to be discussed later. For a very deep cavity (L/D = 1.19), a more stable temperature history is obtained and the cool ring, with relatively larger size but with a slightly smeared downstream edge, can be observed again (Fig. 3f).

In order to compare different cases, attention is focused on a single point on the nose (see Fig. 4). This point (point 2 or P2) is chosen (at about 33 deg from the model axis) to be within the cool ring, which is immediately downstream of the cavity lip for cases in which the cool ring is observed. For the baseline case (i.e., spherical nose; no cavity) and other cavity cases without the cool ring, point 2 corresponds to the same location.

Figure 4 shows the normalized temperature histories at point 2 for the baseline case and for several values of L/D for a model with a sharp lip and spherical cavity base. T is the model surface temperature, T_0 is the tunnel stagnation temperature (in K), and T_i is the "initial" temperature at the

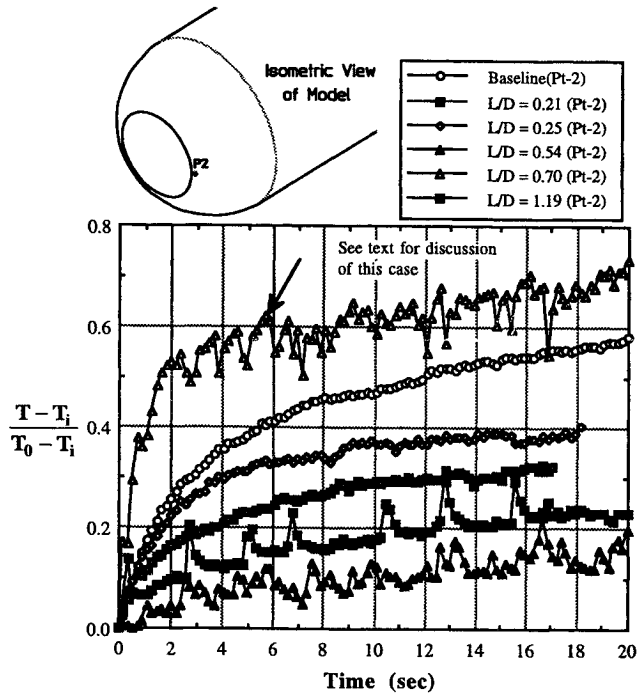

Fig. 4 Normalized temperature histories at point 2 for various cavity depths.

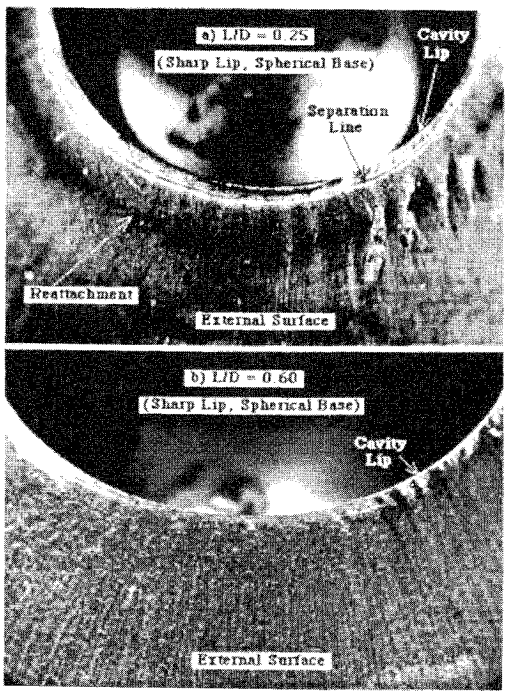

Fig. 5 Flow visualization images, L/D = a) 0.25 and b) 0.60.

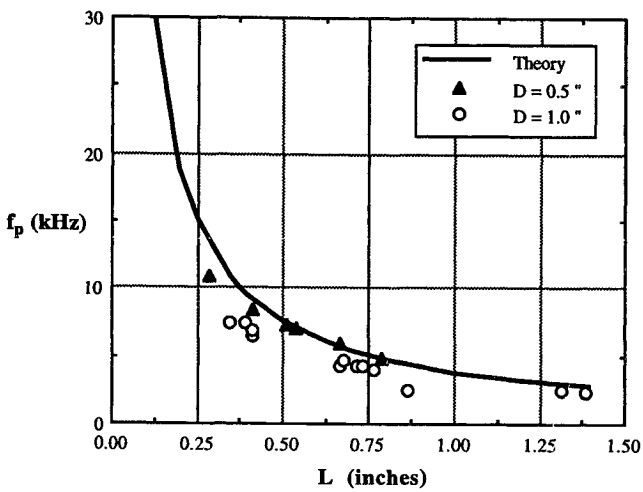

Fig. 6 Experimental and theoretical cavity frequencies.

measurement point. This normalization will be used in temperature history plots throughout this article. The case L/D = 0.25 in Fig. 4 is from the earlier study of Ref. 8. Except for one case (L/D = 0.70), all cases show temperature reduction in the vicinity of the cavity lip. The IR images show that in shallow and very deep cavity cases, this is due to the cool ring. One particular case, L/D = 0.54, in which no cool ring is observed, also shows substantial reduction in surface temperatures that are quite unsteady as can be seen from the figure. A repeat run of this case (not shown) shows similar behavior. In contrast to this case, L/D = 0.70 has higher temperature values. As mentioned above, flow within the deep cavity range is not axisymmetric, and in this particular case point 2 corresponds to a hot spot at the cavity edge, which causes the measured temperature to be relatively higher. For a much deeper case (L/D = 1.19) the temperature history at point 2, falls below the baseline case, again because of a cool ring. Although this case shows peaks in temperature at almost regular intervals a repeat run (not shown), which also has the cool ring, has more frequent troughs and peaks at shorter intervals. However, as is evident in IR images (Fig. 3f) the flow regains its axisymmetric characteristics.

Figure 5a shows a surface flow visualization image for a shallow cavity (L/D = 0.25) with sharp lip and spherical base. Note that the figure shows only half of the cavity viewed normal to the cavity edge. Very close to the cavity lip is the separation line identified by converging surface streak lines. Further downstream is the reattachment line that appears as a dark ring. The extent of this circumferential flow separation correlates approximately with that of the cool ring observed with shallow cavities. Figure 5b shows the flow visualization image for a deep cavity (L/D = 0.60, sharp-lip, and spherical base). In this case, there is no indication of separation and reattachment lines.

All of the cavity configurations exhibit oscillatory flow due to resonance inside the cavity. Most of the energy of the oscillations is at the lowest distinctive frequency, which is considered as the primary resonance frequency. The primary resonance frequency can be calculated from simple linear theory given the cavity depth and the speed of sound inside the cavity. In classic organ pipe mode the wavelength λ_1 of the primary resonance is given as $\lambda_1 = 4L$, where L is the cavity depth. Thus the frequency f_1 corresponding to this wavelength can be obtained knowing the speed of sound a. Assuming that the gas temperature inside the cavity is approximately the stagnation temperature T_0 of the flow $f_1 = a/\lambda_1$, where $a = \sqrt{\gamma RT_0}$. Combining these relations, $f_1 = \sqrt{\gamma RT_0}/4L$ is obtained where γ is the ratio of specific heats and R is the specific gas constant.

Since the flow between the shock and the cavity base oscillates, the appropriate value of L is the distance from the mean location of the bow shock to the cavity base, rather than from the lip to the cavity base. For the baseline case the shock standoff distance is about $0.08D$, so as a first-order approximation this distance has been added to all physical cavity depths. Figure 6 shows the measured frequencies compared to the predicted values. Since cavity diameter is not considered, the agreement with the measurements is poorer for shallower cavities. However, the experimental trend is the same as the theory, and furthermore, excellent agreement between experiment and theory is obtained for very deep cavity cases.

Figure 7 shows sample pressure signals measured at the base of the cavity. Shallow cavity (L/D = 0.25) pressure signals are qualitatively similar to the baseline case with small rms values (1.15% of the freestream pitot pressure P_{t2}), although their power spectra reveal certain resonance frequencies in which the energy is concentrated, unlike the baseline spectrum that is broadband. Further, essentially all data records are similar, indicative of one mode of oscillation.

In contrast, deep cavity (L/D = 0.60) pressure signals are characterized by random switching between two modes that have different amplitudes, but similar frequencies. Signals from all three locations (channels 1, 2, and 3) on the base often have similar behavior, although it is worth noting certain characteristics of the transition to high-amplitude oscillations. The high-amplitude mode starts with decreasing pressure levels on channel 1 and increasing levels on channel 3 (e.g., around 3 ms). Pressure levels on channel 2 are usually between those on channels 1 and 3. This imbalance of the pressure field might either be a triggering mechanism for high-amplitude oscillations, or is a result of a nonaxial oscillation mode perhaps involving radial, or slosh modes. Before returning to the low-amplitude mode all three channels experience similar oscillations, which might indicate that the pressure wave inside the cavity becomes one dimensional towards the end of the high-amplitude mode. This type of oscillation makes the results of standard statistical analysis difficult to interpret in that the overall rms does not truly reflect either condition. It is probable that the lack of flow symmetry and the irregular high-temperature spots observed around the lip in the deep cavity cases are caused by switching between different oscillation modes.

Figure 7 also shows pressure signals for a much deeper cavity case (L/D = 1.19) in which the oscillations become nearly sinusoidal with varying amplitudes. It is evident from Fig. 7 that the rms of pressure oscillations for the shallow cavities is on the order of baseline case values. However, for the deep cavity case, characterized by two modes of oscillation with different amplitudes, the overall rms is almost 10 times the shallow cavity case. While the rms of low-amplitude mode is slightly higher than that of shallow cavity case, the rms of the high-amplitude mode can be as high as 15 times that of shallow cavity case. The rms returns to a smaller value for the very deep cavity case (L/D = 1.19).

Effects of Geometrical Changes

Changes in Lip Geometry

Since flow separation around the cavity edge is the most probable cause of the cool ring in shallow cavity cases, the question of how sensitive the extent of the cool ring is to the changes in lip geometry becomes important. It was anticipated that a rounded lip might reduce or eliminate separation, in turn reducing or eliminating the cool ring.

Figure 8 shows the temperature histories at point 2 for two shallow cavity configurations with sharp and rounded cavity lip (1.5 mm radius). Both cases have spherical cavity bases, but due to different nose pieces, have different L/D values. The legend of this and subsequent figures is such that the first entry in parentheses denotes the L/D value; second, lip shape (SL for sharp lip, RL for rounded lip); third, base shape (SB for spherical base, FB for flat base), and the last is the point at which the measurement is made. The temperature history for the baseline case is also included for reference. As can be seen, rounding the lip generates temperatures at point 2 that are close to those of the baseline case. The IR image for this case reveals that the cool ring is either highly reduced or eliminated.

Figure 9 shows temperature histories at the same points for two deep cavity configurations with sharp and round lips. The baseline case is also shown. Note that the case with the sharp lip is the one that has the lowest temperatures in Fig. 4. As mentioned earlier, this case does not exhibit a cool ring and the temperature history is unsteady compared to shallow cavity or baseline cases. Rounding the lip has a similar effect as in the shallow cavity case. There is also a slight increase in the amplitude of the fluctuating temperature levels, although the cavity depth, which is an important parameter in fluctuating pressures, is approximately 10% smaller due to rounding (see legend) and may be the underlying cause. The temperature histories in Fig. 10 show that rounding the lip reduces or eliminates the cool ring in the very deep case as well.

Figure 11 shows the power spectra of pressure signals measured at the center of the spherical base for shallow cavities with sharp and rounded lips. The power spectrum of the baseline case is also included for comparison. It can be seen in the figure that the rounded lip case has slightly lower energy at the primary resonance frequency than the sharp lip case

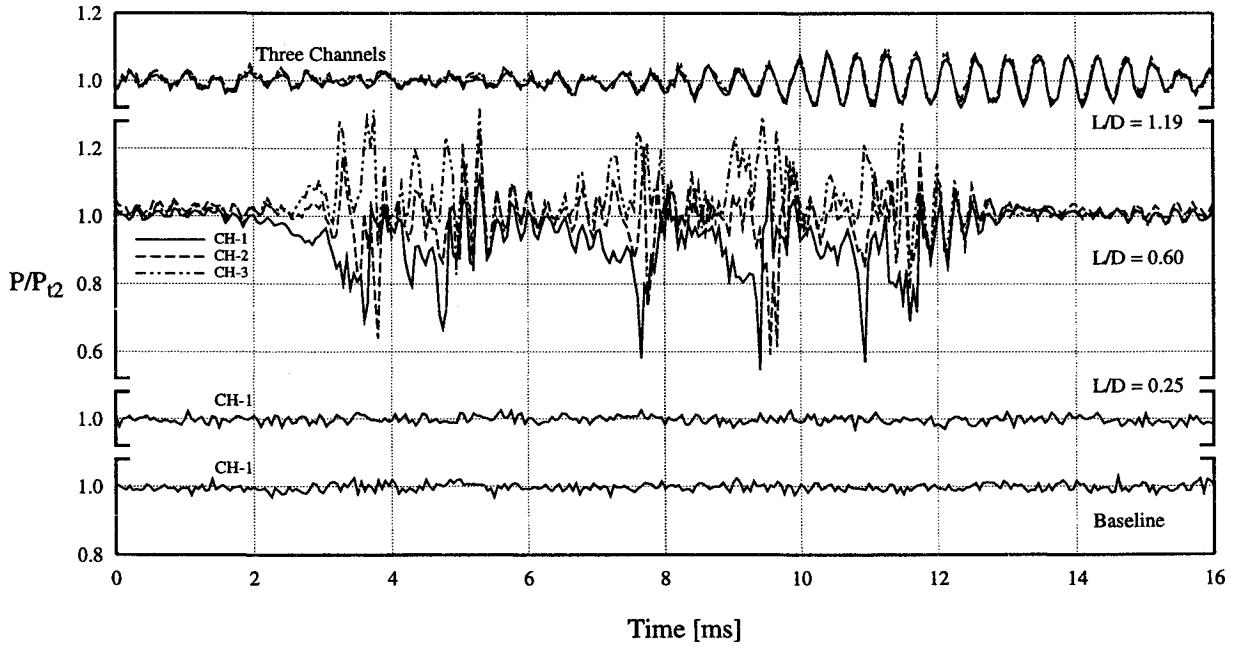

Fig. 7 Sample pressure signals at cavity base for baseline and various cavity cases (L/D = 0.25, 0.60, and 1.19).

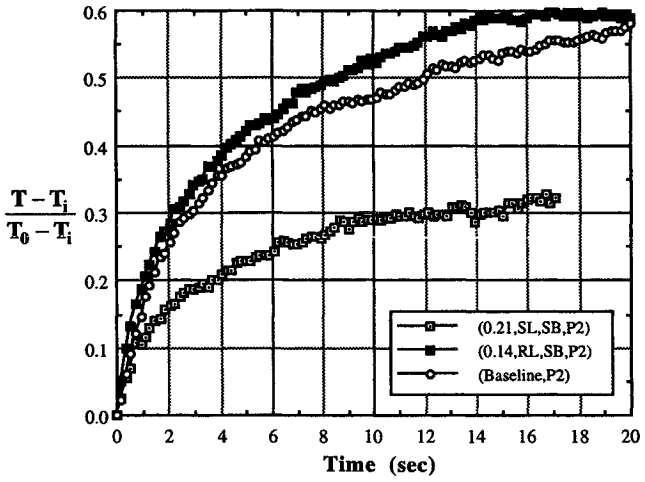

Fig. 8 Effect of cavity lip shape on normalized temperature history (shallow cavities).

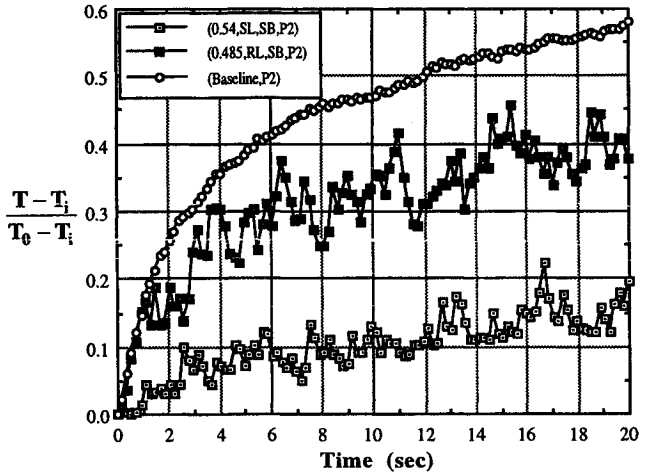

Fig. 9 Effect of cavity lip shape on normalized temperature history (deep cavities).

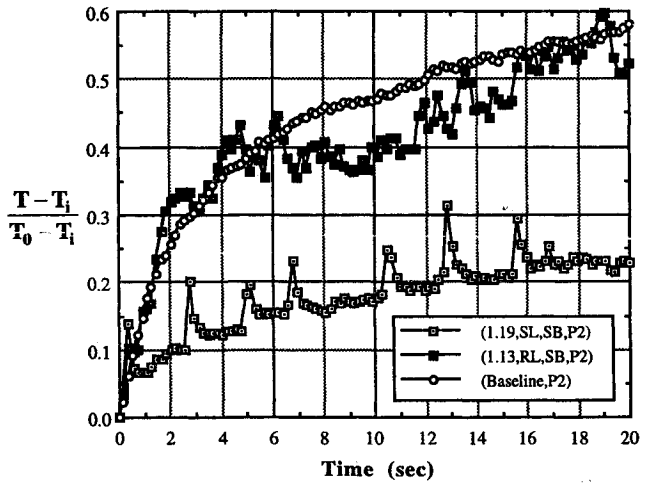

Fig. 10 Effect of cavity lip shape on normalized temperature history (very deep cavities).

due to its lower rms (~5% lower). Note that the small shift to higher values in primary resonance frequency is due to the smaller depth of the rounded lip case. Another observation from examination of off-center spectra (not shown) is the elimination of oscillations at higher harmonics that are present at the center transducer.

Flow dynamics near the cavity base are not substantially affected by changes in the lip shape as can be seen in the cross

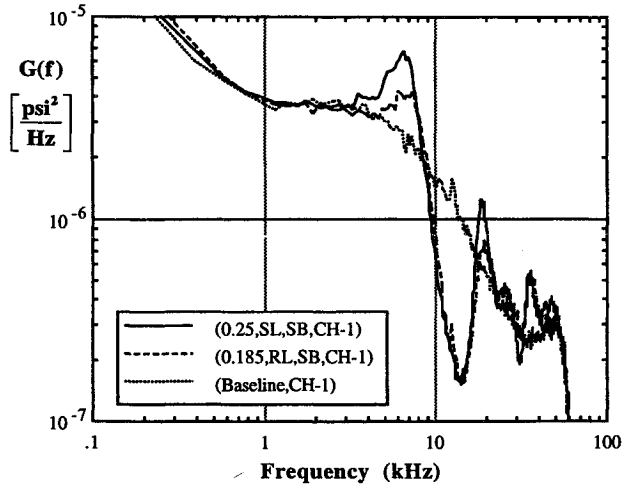

Fig. 11 Effect of cavity lip shape on power spectra at cavity base for shallow cavities (channel 1, base center).

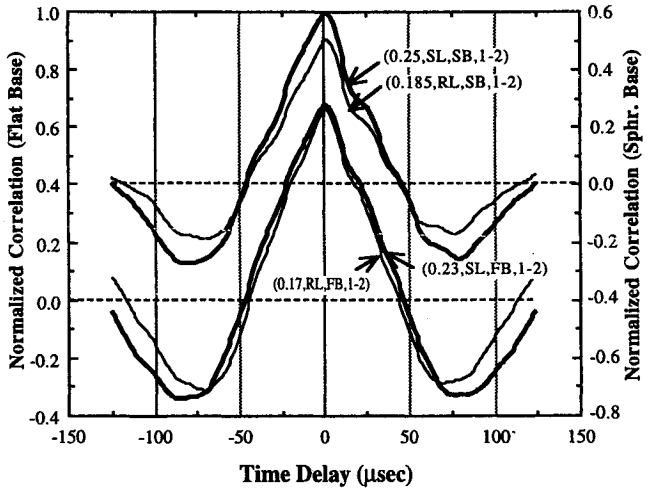

Fig. 12 Effect of cavity lip shape on cross correlations at cavity base for shallow cavities (correlating channels 1 and 2 for spherical and flat bases).

correlations of channels 1 and 2 in Fig. 12. In this case the transducers lie along a vertical line. The cross correlations for the other channel pairs (not shown) also have a maximum at zero time delay, which indicates a relatively planar pressure wave. The cross correlations for shallow cavities with a flat base are also shown in Fig. 12. In this case, there is virtually no difference between sharp lip and rounded lip. However, in the spherical base case, the cavity with a rounded lip has a slightly lower maximum cross-correlation coefficient than that with a sharp lip.

As the cavity becomes deeper, the dynamics of the flow inside the cavity change significantly as seen in the sample pressure signals. This is evident in power spectra for the sharp and round lip in that there is high energy at low frequencies (Fig. 13), which may be a consequence of the random switching from low-amplitude to high-amplitude modes. Figure 13 also shows that by changing the cavity lip shape, there is virtually no change in power spectra of the center transducer signals other than a minor shift in primary resonance frequency due to the smaller depth of the rounded lip case. For off-center channels (not shown) there are small differences especially at lower frequencies, but the general characteristics of the power spectrum are the same. Cross correlations of pressure signals from channels 1 and 2 (Fig. 14) show that signals for the rounded lip have a lower correlation coefficient than for the sharp lip case. Furthermore, cross correlation of off-center channels (2 and 3, not shown here) gives maximum

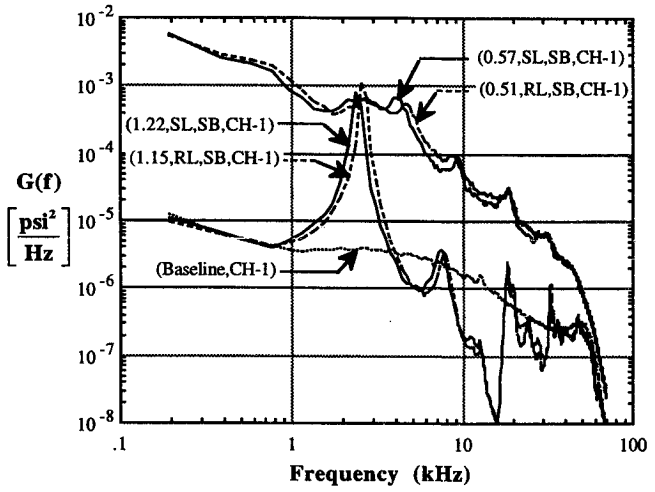

Fig. 13 Effect of cavity lip shape on power spectra at cavity base for deep and very deep cavities (spherical base, channel 1).

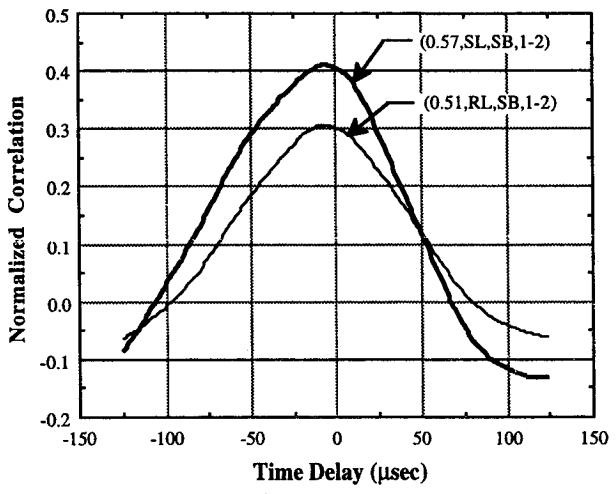

Fig. 14 Effect of cavity lip shape on cross correlations at cavity base for deep cavities (spherical base, channels 1 and 2).

cross-correlation coefficients at different time delays in sharp and rounded lip case with the former being at positive time delay and the latter being at negative time delay. Such results clearly bring out the nonaxisymmetric characteristics of the deep cavity case regardless of the lip shape.

As the cavity depth becomes much larger (very deep cavity), pressure oscillations inside the cavity resemble well-defined sine waves regardless of the lip geometry, as can be seen in power spectra in Fig. 13. Again, the slight shift in primary resonance frequency is due to the shorter length of rounded lip case. Other than that there is almost a perfect match in power spectra, showing that at these depths, cavity lip shape does not influence the pressure fluctuations at the cavity base.

Changes in Base Geometry

There is no significant effect of base shape on the temperature histories for shallow cavities (not shown) other than the minor changes in the rounded lip case due to decrease in effective cavity depth. On the contrary, Fig. 15a shows a substantial increase both in mean and the amplitude of the fluctuating temperature levels for deep cavities with a sharp lip when the cavity base is flat. This might be due to the increase in effective cavity depth with a flat base since it is within this range of L/D that the unstable flow behavior is

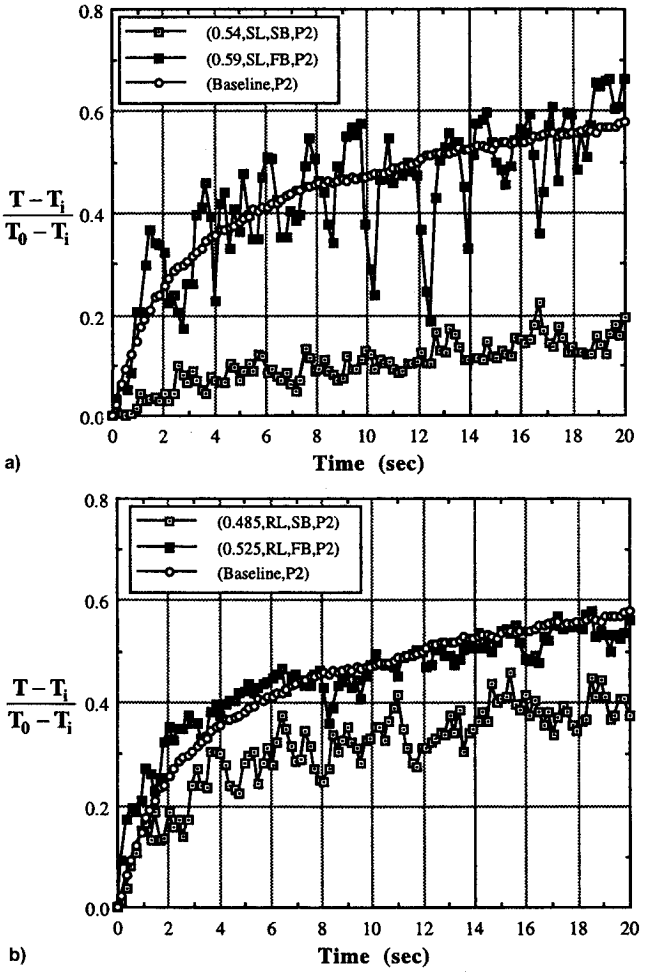

Fig. 15 Effect of cavity base shape on temperature histories for deep cavities: a) with a sharp lip and b) with a rounded lip.

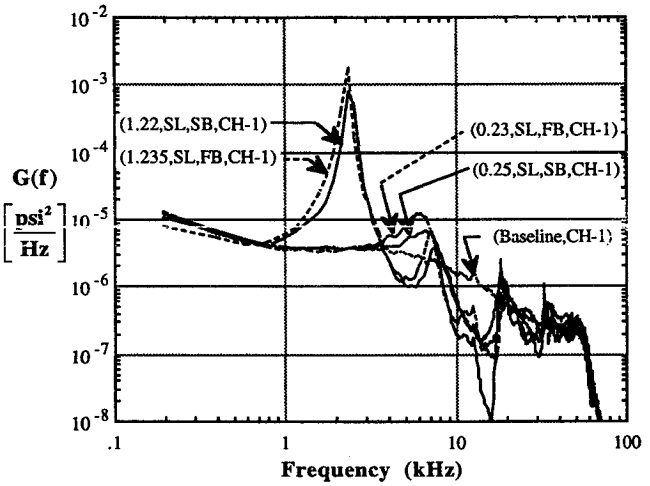

Fig. 16 Effect of cavity base shape on power spectra for a shallow and very deep cavities with a sharp lip (channel 1).

seen. Note that the small difference in L/D values between the spherical and flat base cases (see legend) is due to the very small difference of physical lengths of base pieces used. When the cavity lip is rounded (Fig. 15b) the difference in temperature histories becomes smaller and the flat base case exhibits slightly steadier behavior than the spherical base.

Power spectra (Fig. 16) show a slight increase in energy levels at lower frequencies and a slight decrease at higher

frequencies for the flat base. The slight shift of the primary resonance frequency to lower values is again due to the larger depth of the flat base case. The cross correlations for the same cases (not shown) exhibit a slightly higher value (typically 5%) for the maximum cross-correlation coefficient for the flat base in all the correlation pairs. This might be due to the installation of all three transducers flush with the base in the flat base case, unlike the spherical base in which off-center transducers cannot be installed in such a way. Overall, the differences appear minor.

The effect of base shape on the flow dynamics for very deep cavity cases was also examined. Due to the large depth, there is virtually no change in power spectra (Fig. 16) other than the small shift in frequencies, which is due to different cavity depths of spherical and flat base cases.

Conclusions

Surface temperatures on a hemisphere–cylinder body with a nose cavity in a Mach 4.9 airflow have been measured using an IR camera. Fluctuating surface pressures have also been measured at the cavity base. The cavity diameter D was fixed at one-half the cylinder diameter and the length L of the cavity was varied. If the cavity lip is sharp and the cavity is shallow ($0.15 \leq L/D \leq 0.35$) or very deep ($L/D \geq 1$), an axisymmetric, nominally steady cool ring forms on the external surface downstream of the lip. Flow visualization shows that the cool ring is caused by separation at the lip. Rounding the cavity lip eliminates or reduces separation and temperatures return to levels characteristic of the model without the cavity. For intermediate deep cavities ($0.40 \leq L/D \leq 0.70$), the cavity pressure signals switch from a low-amplitude to high-amplitude level at random intervals, resulting in an unstable, nonaxisymmetric temperature field downstream of the lip. Changes in cavity base shape from spherical to flat have little effect on the temperature history for shallow and very deep cavities, whereas for intermediate depth cavities the effects are more significant.

Acknowledgments

Support for the project was provided in part by the Institute for Advanced Technology, University of Texas at Austin under ARDEC Contract DAAA21-93-C-0101. The authors are grateful to the Center for Energy Studies of the University of Texas at Austin for loan of the infrared camera system. The suggestions of Dennis Wilson are also gratefully acknowledged.

References

[1]Hohler, V., and Stilp, A. J., "Long Rod Penetration Mechanics," *High Velocity Impact Mechanics*, edited by Jonas A. Zukas, Wiley, New York, 1990, Chap. 5.

[2]Baker, J., and Williams, A., "Hypervelocity Penetration of Plate Targets by Rod-Like Projectiles," *International Journal of Impact Engineering*, Vol. 5, Nos. 1–4, 1987, pp. 101–110.

[3]Burbank, P. B., and Stallings, R. L., "Heat-Transfer and Pressure Measurements on a Flat-Face Cylinder at a Mach Number Range of 2.49 to 4.44," NASA TMX-221, Oct. 1959.

[4]Huebner, L. D., and Utreja, L. R., "Experimental Flowfield Measurements of a Nose Cavity Configuration," Society of Automotive Engineers, SAE Paper 871880, Warrendale, PA, Oct. 1987.

[5]Sambamurthi, J. K., Huebner, L. D., and Utreja, L. R., "Hypersonic Flow over a Cone with Nose Cavity," AIAA Paper 87-1193, June 1987.

[6]Marquart, E. J., Grubb, J. B., and Utreja, L. R., "Bow Shock Dynamics of a Forward-Facing Nose Cavity," AIAA Paper 87-2709, Oct. 1987.

[7]Huebner, L. D., and Utreja, L. R., "Mach 10 Bow-Shock Behavior of a Forward-Facing Nose Cavity," *Journal of Spacecraft and Rockets*, Vol. 30, No. 3, 1993, pp. 291–297.

[8]Yuceil, B., Dolling, D. S., and Wilson, D., "A Preliminary Investigation of the Helmholtz Resonator Concept for Heat Flux Reduction," AIAA Paper 93-2742, July 1993.